Colloid Polym Sci (2008) 286:97–106
DOI 10.1007/s00396-007-1752-3

ORIGINAL CONTRIBUTION

In situ fabrication of polyacrylate/nanozirconia hybrid material via frontal photopolymerization

Yanyan Cui · Jianwen Yang · Yunfang Zhan · Zhaohua Zeng · Yonglie Chen

Received: 13 March 2007 / Revised: 22 July 2007 / Accepted: 26 July 2007 / Published online: 18 August 2007

Abstract Frontal photopolymerization was applied to fabricate polymer/nanozirconia hybrid material by using acrylates as polymerizable components and tetrabutyl zirconate (TBZ) as the precursor of nanozirconia, respectively. The nanozirconia particles were in-situ generated with the polymerization front traveling and gradiently dispersed in the simultaneously formed polymer rod. The iodonium salt was utilized as photoacid generator to produce protonic acid and drive TBZ into nanozirconia particles. With the frontal polymerization traveling downward, the particle size and concentration of zirconia increased, but layer-resolved conversion of TBZ decreased. The particle size of zirconia could be reduced remarkably by the protection of monoalkyl titanate bearing six long chains. The refractive index of the hybrid rod was found to increase from top to down. The top–down layer-resolved storage modulus of the hybrid rod increased due to nanoparticle filling effect but decreased beyond the depth of 4 cm from the top, which may be ascribed to particle aggregation.

Keywords Frontal photopolymerization · Organic–inorganic hybrid · Photoacid generator · Zirconia · Nanoparticle

This project is supported by the National Natural Science Foundation of China (grant no. 20304019, 60378029).

Y. Cui · J. Yang (✉) · Y. Zhan · Z. Zeng · Y. Chen
Institute of Polymer Science, School of Chemistry and Chemical Engineering, Sun Yat-Sen University,
Guangzhou 510275, China
e-mail: cesyjw@mail.sysu.edu.cn

Introduction

The investigations of organic/inorganic hybrid nanocomposite have received much attention in the field of material science [1, 2]. The synergism of components in hybrid materials not only combines the distinct properties of organic and inorganic components at a molecular level dispersion, but also gives opportunities to design novel functional materials with some unexpected performance. Therefore, it may find extensive applications to generate functional materials, such as high-refractive-index material [3, 4], nonlinear optical material [5, 6] and waveguide material [7, 8]. Sol–gel process is one of the widely employed techniques for the manufacture of organic–inorganic hybrid material [9]. However, the nanozirconia-based hybrid material, which is attractive in optical and mechanical performance, encounters trouble while traditional sol–gel technique is employed. The precursor, tetraalkyl zirconate, is known to hydrolyze so rapidly that the control of hydrolysis and polycondensation reactions is the key issue for the synthesis of nanocomposites. The prefabricated zirconia sol, even stabilized chemically, is prone to aggregating while slowly thermally curing with organic matrix. UV curing is a fast curing technique that can instantly immobilize the sol particles and prevent them from congregating kinetically. However, great amount of solvent and steric protective agent are indispensable to stabilize the sol dispersion and usually lead to some undesired impacts on the UV-curing process and/or the performance of the cured hybrid composites. Thus, the in situ generation of nanocomposite, which avoided the use of solvents, was proposed for preparing organic–inorganic hybrid materials [10, 11]. Chen and coworkers [4] prepared a hybrid material with high refractive index via in situ process of titanium butoxide with trialkoxysilane-capped

poly(methyl methacrylate). Other interesting methods for producing nanocomposite hybrid include in situ monomer polymerization with the monomer growth of polymer chains from immobilized initiators [12].

Recently, frontal polymerization (FP), a new technique for producing bulk polymer without solvent, has been reported for constructing polyurethane–nanosilica hybrid composite using amino-modified nanosilica particle as cross-linking agent [13]. As a new reaction mode of converting monomer into polymer via a localized and propagating reaction zone, FP was first discovered by Chechilo et al. [14]. Pojman [15] later extended the FP method and rediscovered this phenomenon at ambient pressure in conventional glass tube. The primary nature of traditional FP is that the external heating source, applied on the end of reaction tube to start the polymerization, could be removed after the polymerization zone formed and self-propagated. A lot of effort has been paid to the fundamental investigation and application development of FP. Some functional gradient materials (optic materials) [16], inter-penetrating polymer networks [17], hydrogel [18], and new process for in situ reinforcement of porous materials [19] have been developed via FP.

Photoinitiated polymerization as an efficient, controllable, and nonsolvent synthesis technique has been widely applied in fast manufacture of materials including nanocomposites. Traditionally, photopolymerization was used for thin-film system due to the limited penetration of incident UV light in bulk systems. Fortunately, the photobleaching initiation system permitted the effective penetration of incident UV/visible light. Frontal photopolymerization (FPP) based on the photobleaching mechanism of methylene blue/sodium toluene sulfinate was first mentioned as early as 1994 [18] and became an attractive research topic thereafter [20, 21]. It should be noticed that FPP is a different method from thermal (TFP) and isothermal frontal polymerization (IFP). No matter what kind of frontal polymerization, the primary nature of frontal polymerization is that there exists a narrow polymerization zone, namely polymerization front, in the reactor and travels steadily throughout the reactor from one end to another. The external heating source could be removed after the frontal polymerization is ignited for the TFP process. The polymerization front could spontaneously travel forward with the huge exothermic effect generated by the rapid free radical polymerization of monomer in vicinal reaction layer. Actually, the original driving force for the TFP is the heat-sensitive initiator contained in the reaction system, which is prone to fragmentation and produces primary free radical to initiate polymerization. For the other TFP systems based on none-initiator mechanism, such as isocyanates/polyol, epoxy/hardener, etc., the polymerization can be accelerated by the heat released from itself. IFP, which is also known as interfacial gel polymerization, is initiated by introducing a polymer piece. The polymer piece dissolves and forms a viscous gel region that controls the polymerization rate locally—an effect termed gel effect [22, 23]. It would take couple of hours to complete front traveling for IFP due to low polymerization rate and temperature control. FPP is greatly different from the heat-driving frontal polymerization. For the FPP in this work, the polymerization was only initiated by actinic excitation, and the front was driven forward by the continuous light flux. The reaction front would stop traveling if the incident light was turned off. However, the temperature increasing in front zone due to rapid polymerization is beneficial for speeding up front traveling through accelerating chain propagation and intensifying the Rayleigh–Taylor effect. In a typical comparison, the classic TFP will not stop traveling after ignited, but the FPP could be controlled by the on/off of light flux.

With photopolymerization, temperature of propagation front may be lowered down to a moderate level so that the defects of large hollow, Rayleigh–Taylor effect and convection could be avoided or decreased. Many fundamental aspects of FPP has been investigated or under consideration. Influence of gravity on the behavior of FPP has been investigated by Briskman et al. [24, 26], Righetti et al. [25], and Briskman [27, 28]. Penetration of light flux in the bulky reaction system is an important precondition for FPP. Using photobleachable photoinitiator in the FPP system, the instantly formed polymer matrix in tube would get transparent layer by layer as exposed to proper irradiation [29]. On the basis of Lambert–Beer's law and the photobleaching behavior of the initiator, the spatiotemporal light intensity in the FPP reaction tube has been simulated by Terrones and Pearlstein [30]. Recently, FPP was provided as a means to the fabrication of photolithography of microcircuits, dental restorative, and other biomedical materials [31, 32]. This method also gave a way to rapidly generating multilevel patterns [26, 33].The interest in the present work was to explore the application of FPP in fabricating hybrid optical materials.

Experimental

Materials

Tetrafunctional polyester acrylate (PEA, Acros Actilane 505), tetrabutyl zirconate (TBZ, Aldrich) were used as received. Isobornyl acrylate (IBOA) was obtained from Eternal Chemical by courtesy. Diarylionium salts [Irgacure 250, a 75% solution of (4-methylphenyl)-4-(2-methylpropyl)phenyl iodonium hexaflourophosphate in propylene carbonate] and 2,4,6-trimethylbenzoyldiphenylphosphine oxide (TPO) was obtained from Ciba. Isopropyl tri(dioctyl)

pyrophosphato titanate (TTPO, NDZ-201), a monofunctional titanate coupling agent, was obtained from Nanjing Shuguang Chemical Company. 2-Hydroxyethyl methacrylate (HEMA, Mitsubishi Chemical) was dried over 4A molecular sieve before use.

Preparations of the hybrid materials

In a typical experiment, 0.1 g of TPO was fully dissolved to 2.5 g IBOA to form a clear solution, and then 4.1 g PEA was added to get a transparent viscous solution. The second solution composed of 0.05 g Irgacure 250 and 0.5 g HEMA was added dropwise to the former viscous solution and then mixed with the third solution of 1.0 g TBZ and 2.5 g IBOA by vigorous stirring. The obtained solution was filled into a 9×100-mm glass tube encased with a rubber bulb at the bottom to compensate polymerization shrinkage. A Phillips medium pressure mercury lamp (125 W) that emitted ultraviolet light in high efficiency was employed to irradiate the filled tube overhead (Scheme 1).

In the modified synthesis of hybrid rod by FPP, the protective agent, TTPO, was added into the aforementioned initial FPP sample to control the particle size of in situ generated nanozirconia.

Characterization

The light intensity for exposure was measured with an UV-A radiometer (sensitive in the wavelength range of 320–400 nm). Fourier transform infrared (FT-IR) spectra were recorded on a Nicolet Nexus-670 infrared spectrometer. KBr pellet was used as the background. The morphology observation of the hybrid product was conducted on a JEOL JSM-6330F scanning electron microscope (SEM) after the sample rod was fractured in liquid nitrogen. A JEM-2010 (HR) transmission electron microscope (TEM) was adopted to investigate the shape and distribution of zirconia particles in the hybrid material. A TA/DMA 2980 dynamic thermomechanical analyzer (DMA) was used to determine the mechanical property of the sliced composite rod from −30 to 80 °C with a heating rate of 2 °C/min and a frequency of 1.0 Hz under nitrogen atmosphere. Refractive index was obtained with a 2 WA-J Abbe refractometer. The temperature profiles of the FPP process was monitored with a set of tiny thermocouples (model WRNK-191S, φ 1.0 mm) that were inserted through the plastic pipe wall and contacted with the reaction substrate. All of the installed thermocouples were connected with digital multimeters (DT9508B, Shenzhen Hongda Electronic, China), and the shown temperature data changing with irradiation time were recorded by video camera (shown in Scheme 2).

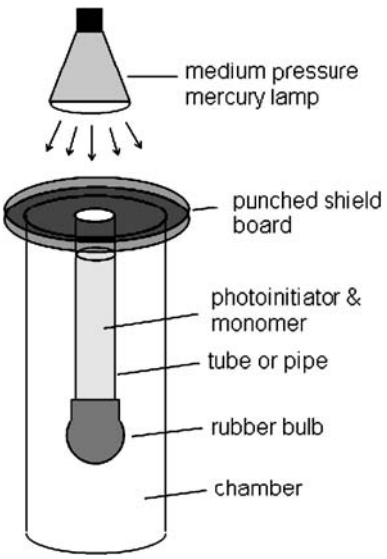

Scheme 1 Schematic diagram for descending FPP

Results and discussion

The spatiotemporal kinetics is a primary important aspect of FPP. Localized polymerization in FPP is usually accompanied with spontaneous temperature increase. The multipoints temperature monitoring was designed in the present FPP study as shown in Scheme 2. Exposing the sample filled pipe to UV light, the temperatures around the four thermocouples would successively increase when the FPP front reached the thermocouples and then decreased slowly after a maximum. The obtained spatial temperature profiles for the hybrid FPP system is shown in Fig. 1.

With the distance of thermocouples and the time between two temperature maxima, the segmented average traveling velocities of the hybrid system were calculated and plotted against tube depth in Fig. 2. For the FPP hybrid

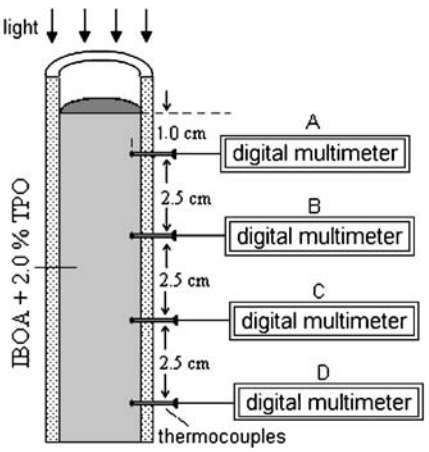

Scheme 2 Installation for the spatiotemporal temperature determination of FPP (light intensity: 2.9 mW/cm^2, tube diameter: 9.0 mm)

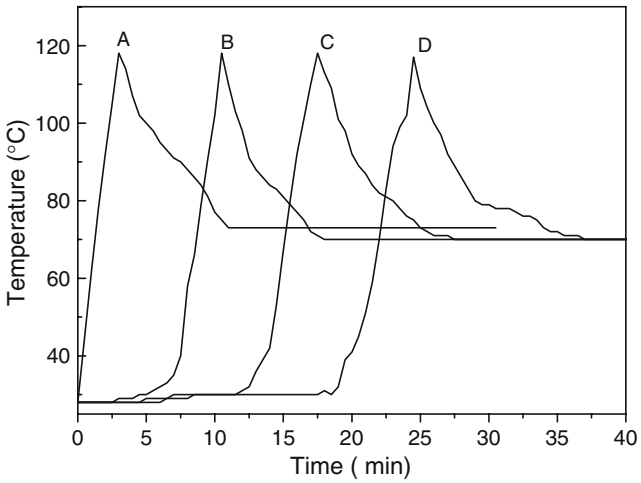

Fig. 1 Temperature profiles for hybrid FPP system (light intensity: 2.9 mW/cm^2)

system, the front traveling velocities got decreased and then improved with the front traveling.

For an ideal FP system, the propagating front is supposed to be a perfect plane, and the front velocity is a constant. However, the front velocity is very complicated and could be affected by many factors, such as photoinitiator, temperature, and monomer structure [34, 35]. Due to the exothermic effect of polymerization, the polymerization fronts advanced ahead accompanied with thermal convection and intensified Rayleigh–Taylor effect within the traveling reaction zone, leading to accelerated speed.

(4-Methylphenyl)-4-(2-methylpropyl) phenyl iodonium hexaflourophosphate (Irgacure 250) is an efficient cationic photoinitiator that could simultaneously generate super acid and free radical under UV irradiation. The photogenerated protonic acid is an efficient activator that could catalyze the hydrolysis of TBZ in the presence of moisture or trace amount water and the subsequent polycondensation of hydroxylated zirconium structure. The photoreleased radical could aid to initiate the polymerization of acrylates, although FPP was primarily initiated by TPO that was a more efficient photoinitiator. Additionally, the iodonium salt has the longest maximum absorption wavelength at 242 nm, which does not perfectly match the main emission lines of the UV lamp. Nevertheless, the free radical fragments produced through the photolysis of TPO at long wavelength (λ_{max}, ~373 nm) could reduce the iodonium salt to accelerate the generation of active cationic species and protonic acid [36, 37]. That is to say, the iodonium photoacid generator with poor absorption matching could be sensitized by the coexisted TPO in some degree. Thus, polyacrylate/inorganics composite containing synchronous formed amorphous zirconia particles were produced along with the advancing of polymerization front (Scheme 3). It could be estimated that the polymerization front traveled in an average rate of about 3.4 mm/min. Due to incomplete polymerization and plasticization of the residual monomer, the bottom end (front section) of polymer rod was too soft to be suitable for subsequent identification.

The obtained polymer rod was cut into small segments in an interval of 10 mm and subjected to FT-IR measurement. A series of IR spectra for the polyacrylates/zirconia hybrid segments are shown in Fig. 3. The absorption band at 1,634 cm^{-1} was assigned to acryloxyl groups, which increased steadily layer by layer (Fig. 3a). It was suggested that there existed a decreased gradient polymerization conversion from top to bottom that could be, of course, ascribed to the absorption of residual TPO in the upper layer to the incident light, reflection or scattering of formed

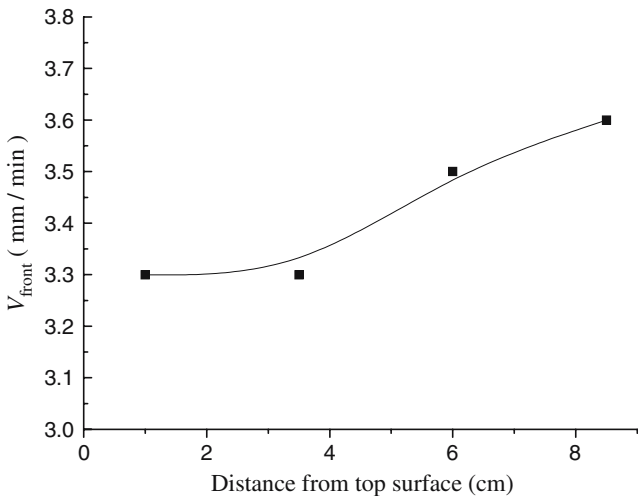

Fig. 2 Average velocities of front traveling vs traveling distance for the F hybrid PP system based on temperature profiles (light intensity: 2.9 mW/cm^2)

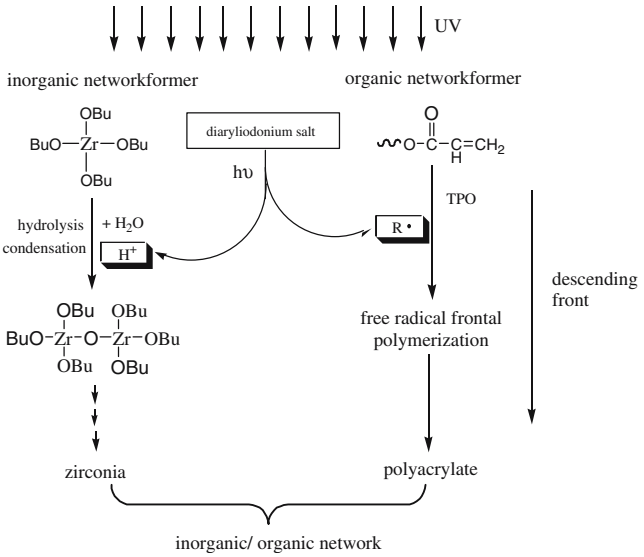

Scheme 3 Dual photoreactions of TBZ and acrylates in FPP process

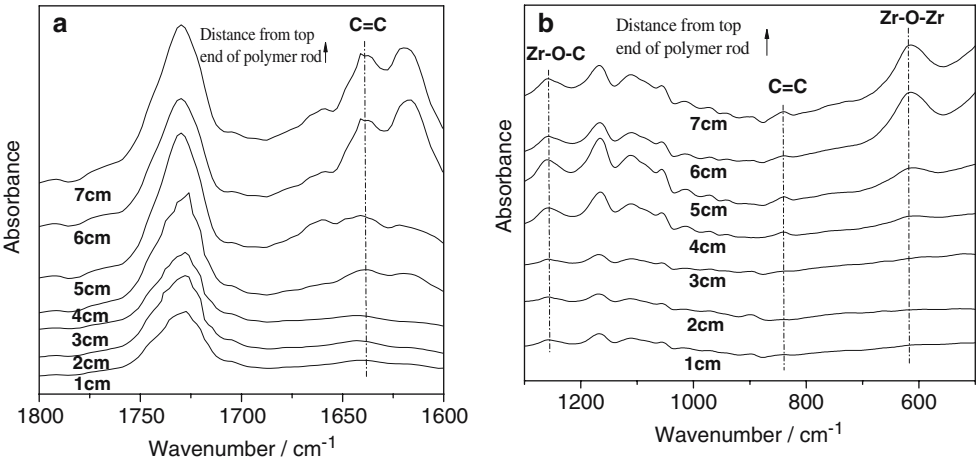

Fig. 3 Spatial FT-IR spectra of hybrid sample rod (**a**) 1,800~1,600 cm^{-1} (**b**) 1,300~550 cm^{-1} (light intensity: 2.9 mW/cm^2, irradiation time: 40 min)

polymer, and the attenuation of light intensity along with the front traveling direction. Another characteristic absorption band around 820 cm^{-1} that was assigned to the twist vibration of $=CH_2$ changed with the same trend (Fig. 3b). The peak at 1,274 cm^{-1} was attributed to Zr–O–C of starting zirconate, and the band at 640 cm^{-1} corresponded to the Zr–O–Zr stretching vibration. The absorption bands at 1,274 cm^{-1} and 640 cm^{-1} were selected to calculate the conversion of Zr–O–C and the concentration of zirconia in hybrid matrix with the carbonyl absorption band at 1,720 cm^{-1} as internal standard. The top–down spatial conversion of TBZ and spatial distribution of zirconia are plotted in Fig. 4.

As shown in Fig. 4, it could be confirmed that the Zr–O–Zr structure was generated with the propagation of polymerization front. In the vertical polymer rod, it was found that the residual TBZ and the resulted zirconia had a top–down distribution. The content of the residual TBZ decreased with sample depth, but the concentration of produced zirconia changed oppositely. Iodonium salt usually exhibits high photoreactivity (photolysis quantum yield), although its absorption wavelength does not match up with the ordinary UV radiation lines perfectly [38]. Theoretically, the iodonium salt in the upper layer was exposed to UV light in higher intensity and then generated more concentrated protonic acid to accelerate the formation zirconia rapidly in contrast to that in the lower layers. However, TPO having efficient absorption at broad spectrum scope would screen iodonium salt and, thus, delayed the photolysis of the latter till the TPO in the upper layer was photobleached. On the other hand, the photopolymerization of acrylates was so rapid that a hard network was formed in the upper layer upon exposing to UV light. The instantly formed acrylic network would immobilize the unreacted TBZ in some degree and blocked the diffusion of substrates that were involved in the reaction of TBZ, such as moisture and iodonium salt. The photoacid that catalyzed hydrolysis and polycondensation of zirconate precursor was limited and lagged behind the formation of acrylic polymer in the same layer while FPP advancing. Due to the poor compatibility of ionic iodonium salt, some fraction of iodonium salt might be squeezed out from the fast-formed acrylic network and concentrated in the lower layer gradually. A simple survey was conducted to follow the change of acidity of the residual substrate below the polymerization front. The FPP process was ceased after a certain irradiation time, and the acidity of the residual

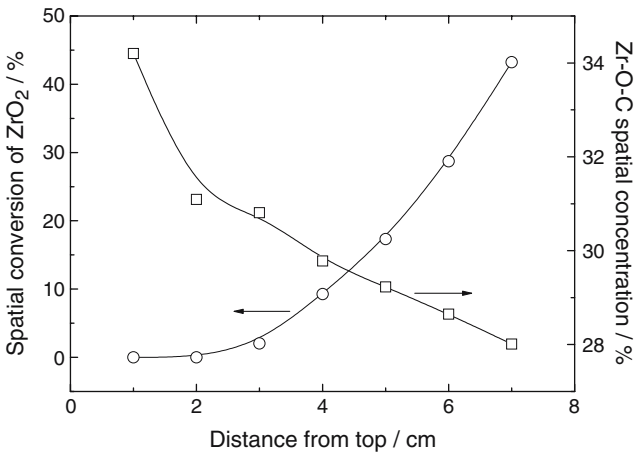

Fig. 4 Spatial conversion of ZrO_2 and conversion of Zr–O–C band (light intensity, 2.9 mW/cm^2; irradiation time, 40 min)

Table 1 The acidity of residual solution after a certain period of irradiation

Irradiation time per minute	pH Number
0	7
9	6
13	4
19	2
22	1
30	1

solution was measured with test paper. The result is shown in Table 1.

There was an accumulation effect for the photogenerated acid according to Table 1. The concentration of photogenerated acid in the unreacted liquid phase increased with sustaining radiation due to the photobleaching of TPO. This result was also consistent with the possible downward migration of iodonium salt from the solid polymer. The increased concentration of acid was of course in favor of the formation of zirconia. Furthermore, TBZ was also found to be incompletely compatible with the formed polyacrylate network. Some fraction of the residual TBZ might immigrate into the liquid phase below so as to be concentrated in the unreacted layer. Thus, it could be understood that more and more inorganic particles should be produced with the polymerization front progresses.

Morphology and microstructure

It had been shown that Zr–O–Zr structure was produced with the depletion of organic zirconate in the FPP process according to the FT-IR spectrum identification. However, it was not enough to indicate the profile and microstructure of the produced inorganic domain in the FPP hybrid rod. As potential optical materials, the domain size and distribution of the inorganic phase in the hybrid system were important and should be controlled during synthesis. Large particles dispersed in continuous organic matrix usually led to Rayleigh scattering and Mie's scattering, which would increase signal loss in optical conduction. SEM was employed to observe the morphology of the brittle fracture surface of the obtained FPP product. Figure 5 is the SEM micrograph for the fracture surface of FPP polymer rod without TBZ and iodonium salt. The striations on the smooth fracture surface might be attributed to the temperature gradient during FPP. Rayleigh–Taylor effect and moderate convection [39] were considered to be the direct factors inducing the oriented striations.

For the FPP hybrid rod, the fracture surface that was 5.5 cm away from the top surface was observed under SEM and the micrograph is shown in Fig. 6 (a and b in different scale). It was indicated that the zirconia particles were dispersed evenly on the whole at the investigated latitude. The particle size was estimated to be 100–200 nm, although some of the particles were partially buried in the organic matrix. The appearance of these particles was not regular enough due to the unfinished aggregation, but they were well separated nevertheless. The hydrolysis intermediate of TBZ, ≡Zr–OH, was so active as to undergo condensation easily. The early formed small particles would rapidly aggregate to large domain unless any protection was taken during the irradiation. By the FPP, the in-situ-generated zirconia particles in certain depth could be immobilized in the hard acrylic network, and serious aggregation could be prevented. It could be recognized that the zirconia nanoparticles was in situ generated and in situ protected by FPP

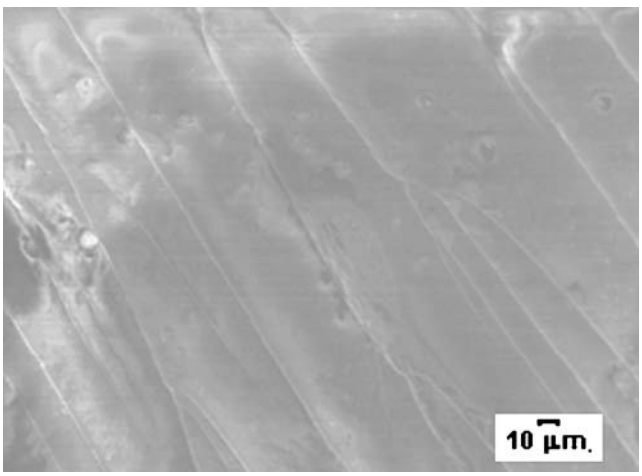

Fig. 5 SEM micrograph for the FPP product in the absence of TBZ (light intensity, 2.9 mW/cm^2; irradiation time, 40 min)

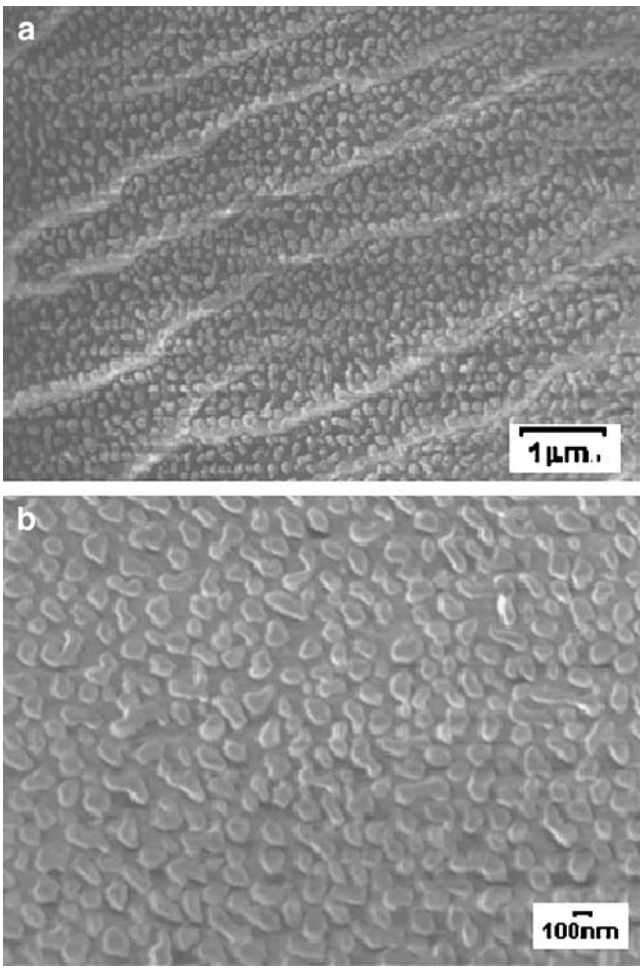

Fig. 6 SEM micrograph of hybrid rod sample (cross-section depth, 5.0 mm; light intensity, 2.9 mW/cm^2; irradiation time, 40 min)

at the same time. Of course, it was absolutely possible that continuous aggregation would occur in the soft polymerization front in which the conversion and cross-linking density were too low to limit the particles. Nevertheless, the particle growth in the soft front section was not fast above certain depth because some fraction of iodonium salt and TBZ would be squeezed out from the section on the basis of limited compatibility, and the local concentration of these substrates decreased.

Frontal polymerization is an effective method to fabricate gradient materials. It had been reported that the polymer with gradient refractive index (GRIN) was synthesized through interfacial-gel copolymerization, which was classified as isothermal frontal polymerization [40]. As described above, there is incident light attenuation in the FPP tube. TBZ and iodonium salt might partially immigrate downward as the polymerization front approaches. Thus, finally, formed zirconia particles also presumably distributed in top–down gradient in the composite rod. The hybrid rod was sliced at three different depth, and the samples were subjected to TEM investigation. The TEM micrographs (Fig. 7) show that the particle morphology changed with sample depth increasing. The particle size at the depth of 2.5 cm was around 30 nm and increased to around 70 nm at the depth of 5.0 cm. At the depth of 7.5 cm, the small primary particles finally stuck to one another and formed large aggregated particle with the observed size of around 800 nm (Fig. 7c). The concentration of zirconia particles also changed with the depth increasing. The in-situ-generated zirconia particles along with the FPP front traveling had a top–down distribution and immobilized in the polymer network. Considering the acidity of residual solution below the front increasing with radiation time and the induced enrichment tendency of TBZ and iodonium salt, the fabrication of gradient hybrid composition by FPP could be understood.

As discussed above, the in-situ-generated zirconia particles grew too rapid and easily reached large size at the far distance from the top. The ≡Zr–OH moieties, which extensively existed on the surface of initially generated small zirconia particles, were so reactive as to condense each other to form Zr–O–Zr bond, and then large particles were produced. It was deficient that the particles were protected only by the in-situ-constructed polymer network, especially for the deep location, at which the primary zirconia particles might be generated in high concentration.

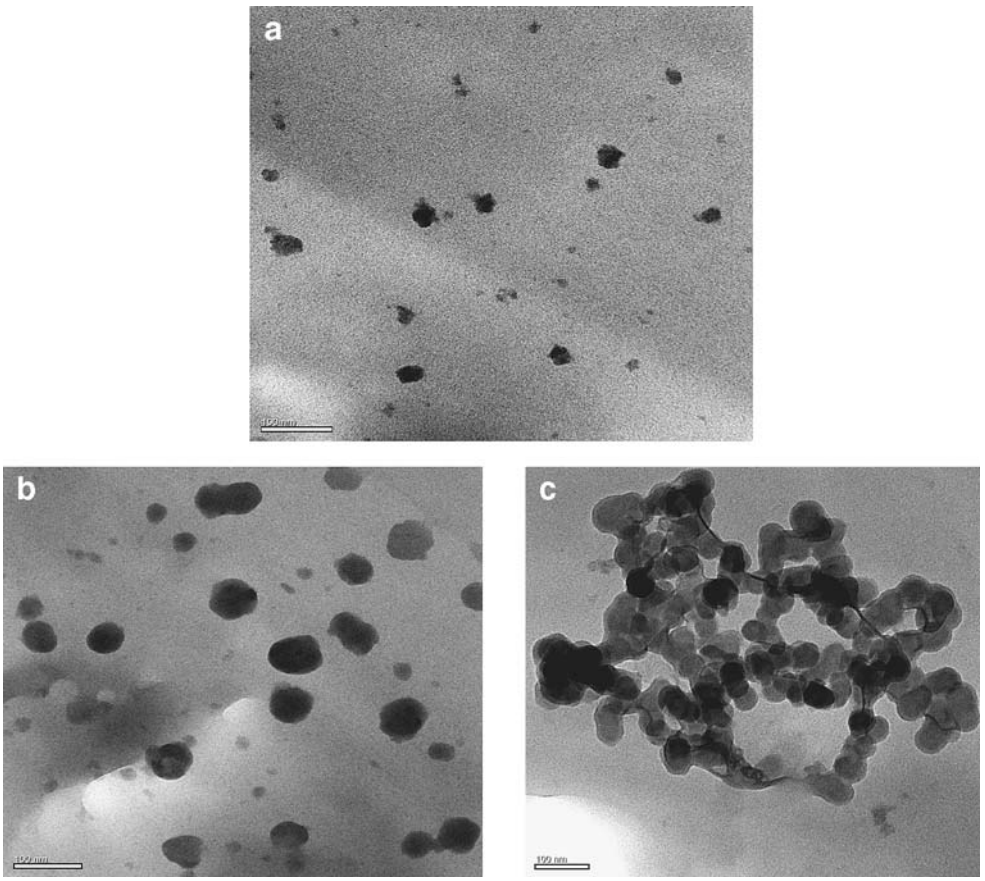

Fig. 7 TEM micrograph of hybrid rod at different depth (scale bar 100 nm; **a** 2.5 cm, **b** 5.0 cm, **c** 7.5 cm (light intensity, 2.9 mW/cm^2; irradiation time, 40 min; scale bar, 100 nm)

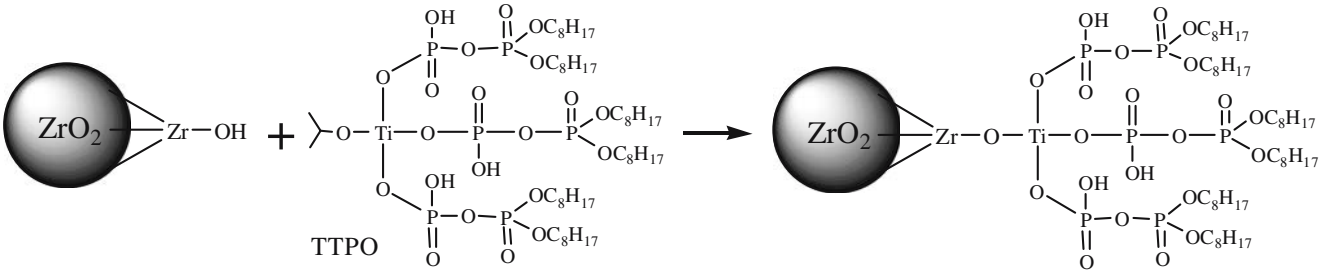

Scheme 4 Surface modification of zirconia nanoparticles by TTPO

Additional protection should be taken to control the morphology of zirconia particles efficiently. TTPO, an efficient monofunctional coupling agent bearing six octyl groups, was used herein to condense with the hydroxylated zirconium moiety, and the octyl groups were attached to the surface of zirconia particles. The protective coupling reaction is shown as Scheme 4.

On the basis of the aforementioned substrates ratio, 0.25 g of TTPO was added to the system for FPP investigation. The obtained hybrid rod was cut at the depth of 5 cm away from the top, and a sliced sample was subjected to TEM observation. As shown in Fig. 8, the particle size at the depth of 5.0 cm was controlled around 20 nm, which was remarkably decreased comparing with that in Fig. 7b. Hydrocarbon long chain was well known to exhibit low surface tension and contributed to poor interfacial adhesion. By coupling the reaction between TTPO and the hydroxylated zirconium moieties on particle surface, abundant hydrocarbon long chains were anchored on the surface to form a protective shell surrounding the zirconia core. The serious congregation between the primary zirconia particles was, thus, prevented with the effective steric hindrance and the low surface energy of the hydrocarbon shell. Actually, the transparency of the hybrid rod in the far deep front (~8–9 cm) was also effectively improved with the protection of TTPO. The bonded hydrocarbon chains will also enhance the compatibility between the acrylic network and the inorganic nanoparticles.

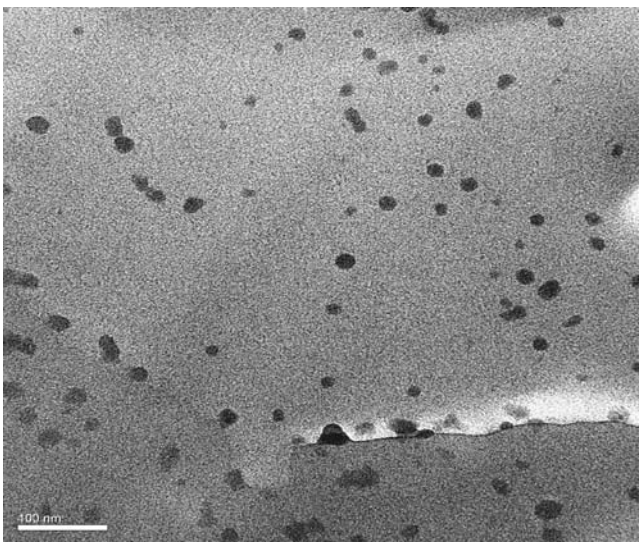

Fig. 8 TEM cross-section micrograph of hybrid rod at 5.0 cm depth, using TTPO as surface modifier (light intensity, 2.9 mW/cm^2; irradiation time, 40 min; scale bar, 100 nm)

Dynamic mechanical analysis

Thermomechanical property is one of the important aspects for optical materials. The gradient distribution of nanozirconia particles in the FPP hybrid rod might lead to gradient thermomechanical property. The obtained hybrid rod was cut into pellets with the thickness of 4 mm, and the pellet samples were subjected to DMA investigation. The depth-resolved DMA curves are shown in Fig. 9. For the hybrid FPP sample, the drop in storage modulus (E') and peak in damping factor (tan delta) between 20 and 60 °C was due to the glass transition (T_g) of the organic polymer phase interacted with the nanozirconia particles. The glass state E' for the hybrid samples was generally improved comparing with net organic FPP polymer. It was also found that the E' for the hybrid FPP samples changed in parabolic style. The E' increased along with the front traveling direction firstly (Fig. 9a) and then decreased (Fig. 9b). The results should be related with the gradient distribution of nanozirconia particles. The inorganic nanoparticles in small diameter usually have huge specific surface and intensively interact with the surrounding hydrophilic groups, e.g., hydroxyl group from HEMA. Well-dispersed nanoparticles in the upper layers were favorable for improving the performance of the composite materials, and the modulus increased with the nanoparticles content. However, serious congregation of the primary nanoparticles in the lower layers that led large particles impaired this enhancement.

The glass transition temperatures were indicated by the tan δ peaks in Fig. 9c and d. The T_g for the hybrid composite

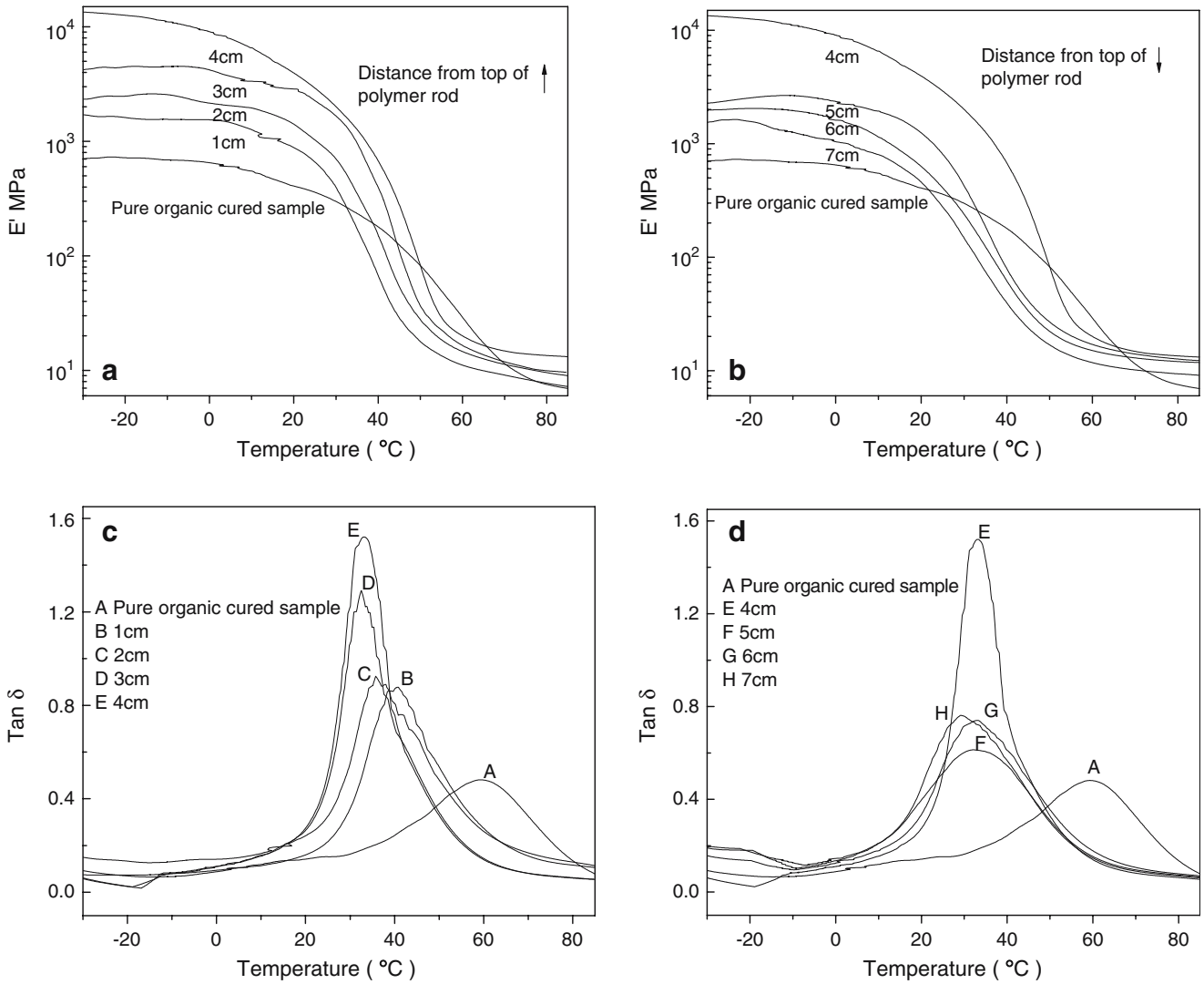

Fig. 9 Spatial dynamic mechanical analysis of ZrO_2/PEA hybrid sample rod (light intensity, 2.9 mW/cm^2; irradiation time, 40 min). *E′* increased along with the front traveling direction (**a**) and then decreased (**b**). **c**, **d** Glass transition temperatures

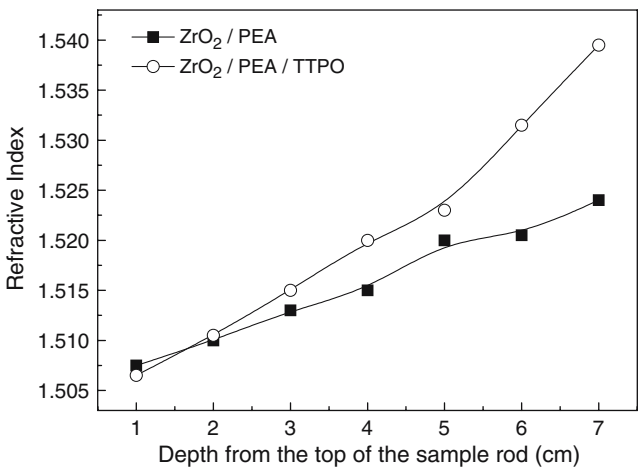

Fig. 10 Refractive index of hybrid rod (light intensity, 2.9 mW/cm^2; irradiation time, 40 min)

was lower than the net acrylic reference. It might be ascribed to the plasticization of residual butanol that was released from TBZ during hydrolysis and polycondensation.

Refractive index variation

The obtained FPP hybrid rod was selectively cut at each centimeter site, and the pellets with the thickness of 1 mm were subjected to refractive index. Figure 10 showed the spatial variations of the refractive index layer by layer of the hybrid rod. The refractive index increased from 1.507 for the first centimeter layer to 1.524 for the seventh centimeter layer. It seemed accordant with the top–down distribution of zirconia content in the FPP rod. With the efficient interaction of TTPO, the refractive index was improved to 1.540 for the seventh centimeter layer due to

the well dispersion of nanozirconia particles. It was revealed that controlled fabrication of the nanoparticles in hybrid materials was important to obtain the high performance.

In the present work, a top–down gradient hybrid rod was fabricated. Based on the same mechanism, a radial gradient rod was also synthesized.

Conclusion

Using the FPP of acrylates in the presence of organic zirconate and iodonium salt, axial gradient polyacrylate/nanozirconia hybrid rod was fabricated. The nanozirconia, in situ generated in the frontal polymerization matrix with the photocatalysis of iodonium salt, was presented with a top–down distribution in the obtained hybrid rod, both in particle size and in particle concentration. A mechanism of induced enrichment of iodonium salt and organic zirconate during FPP process was proposed. The refractive index of the hybrid rod increased along with the front traveling direction and reached 1.540 at the depth of 7 cm from the top.

Reference

1. Schubert U, Hüsing N, Lorenz A (1995) Chem Mater 7:2010
2. Nagarale RK, Gohil GS, Shahi Vinod K, Rangarajan R (2004) Macromolecules 37:10023
3. Wang B, Wilkes GL, Hedrick JC, Liptak SC, McGrath JE (1991) Macromolecules 24:3449
4. Lee LH, Chen WC (2001) Chem Mater 13:1137
5. Jiang H, Kakkar AK (1998) Adv Mater 10:1093
6. Yuwono AH, Xue J, Wang J et al (2003) J Mater Chem 13:1475
7. Bartl MH, Boettcher SW, Hu EL, Stucky GD (2004) J Am Chem Soc 126:10826
8. Yoshida M, Prasad PN (1996) Chem Mater 8:235
9. Mark JE (1995) Some general trends in the area of organic–inorganic composites. In: Mark JE, Lee CY-C, Bianconi PA (eds) Hybrid organic–inorganic composites, vol 585. ACS Symposia ACS, Washington, DC, p 1
10. Tamaki R, Chujo Y (1998) Appl Organomet Chem 12:755
11. Chang CC, Chen WC (2002) Chem Mater 14:4242
12. Timothy VW, Timothy EPJ (1999) Am Chem Soc 121:7409
13. Chen S, Sui J, Chen L, Pojman JA (2005) J Polym Sci A Polym Chem 43:1670
14. Chechilo NM, Khvilivitskii RJ, Enikolopyan NS (1972) Dokl Akad Nauk SSSR 204:1180
15. Pojman JAJ (1991) Am Chem Soc 113:6284
16. Pojman JA, McCardle TW (2000) US Patent 6057406
17. Pojman JA, Elcan W, Khan AM, Mathias LJ (1997) Polym Sci A Polym Chem 35:227
18. Washington RP, Steinbock OJ (2001) Am Chem Soc 123:7933
19. Pojman JA, Warren J (1998) Polym Prepr (ACS Div Polym Chem) 39:356
20. Cabral JT, Hudson SD, Harrison C, Douglas JF (2004) Langmuir 20:10020
21. Decker C, Keller L, Zahouily K, Benfarhi S (2005) Polymer 46:6640
22. Khan AM, Pojman JA (1996) Trends Polym Sci 4:253
23. Lewis LL, Debisschop CA, Pojman JA, Volpert VA (2004) ACS Symp Ser 869:169
24. Briskman VA, Kostarev KG, Lyubimova TP (1994) Plenum, New York, pp 185–192
25. Righetti PG, Bossi A, Giglio M et al (1994) Electrophoresis 15:1005
26. Briskman VA, Kostarev KG, Levtov V et al (1996) Acta Astronautica 39:395
27. Briskman VA (1999) Adv Space Res 24:1199
28. Briskman VA (2001) ACS symposium series no. 793. In: Downey JP, Pojman JA (ed) American Chemical Society, Washington, DC, pp 97–110
29. Ivanov VV, Decker C (2001) Polym Int 50:113
30. Terrones G, Pearlstein A (2001) J Macromol 34:3195
31. Decker C (1998) Polym Int 45:133
32. Decker C (2002) Polym Int 51:1141
33. Warren JA, Cabral JT, Douglas JF (2005) Phys Rev E 72:021801
34. Pojman JA, Willis J, Fortenberry D, Ilyashenko V, Khan A (1995) J Polym Sci A Polym Chem 33:643
35. Nason C, Roper T, Hoyle C, Pojman JA 2005 Macromolecules 38:5506
36. Yagci Y, Schnabel W (1987) Makromol Chem Rapid Commun 8:209
37. Chen ZG, Webster DC (2006) J Polym Sci A Polym Chem 44:4435
38. Timpe HJ, Schikowsky, V (1989) J Prakt Chem 331:447
39. Belk M, Kostarev KG, Volpert V, Yudina TM (2003) J Phys Chem B 107:10292
40. Koike Y, Takezawa Y, Ohtsuka Y (1988) Appl Opt 27:486